Chemical Science

ROYAL SOCIETY OF CHEMISTRY

EDGE ARTICLE

View Article Online
View Journal | View Issue

Cite this: *Chem. Sci.*, 2024, **15**, 1505

All publication charges for this article have been paid for by the Royal Society of Chemistry

Water-promoted selective photocatalytic methane oxidation for methanol production†

Peng Zhou, [a] Songtao Tang,[a] Zhengwei Ye,[a] Ishtiaque Ahmed Navid,[a] Yixin Xiao,[a] Kai Sun[b] and Zetian Mi*[a]

Converting relatively inert methane into active chemical fuels such as methanol with high selectivity through an energy-saving strategy has remained a grand challenge. Photocatalytic technology consuming solar energy is an appealing alternative for methane reforming. However, the low efficiency and the undesirable formation of low-value products, such as carbon dioxide and ethane, limit the commercial application of photocatalytic technology. Herein, we find a facile and practical water-promoted pathway for photocatalytic methane reforming into methanol, enabling methanol production from methane and oxygen with a high selectivity (>93%) and production rate (21.4 μmol cm^{-2} h^{-1} or 45.5 mmol g^{-1} h^{-1}) on metallic Ag nanoparticle-loaded InGaN nanowires (Ag/InGaN). The experimental XPS and theoretical PDOS analyses reveal that water molecules adsorbed on Ag nanoparticles (AgNPs) can promote the electron transfer from InGaN to AgNPs, which enables the formation of partial Ag species with a lower oxidation state in AgNPs. Through the *in situ* IR spectrum and the reaction pathway simulation studies, these newly formed Ag species induced by water adsorption were demonstrated to be responsible for the highly selective methanol production due to the effective formation of a C–O bond and the optimal desorption of the formed methanol from the surface indium site of the InGaN photocatalyst. This unique water promotion effect leads to a 55-fold higher catalytic rate and 9-fold higher selectivity for methanol production compared to photocatalytic methane reforming without water addition. This finding offers a new pathway for achieving clean solar fuels by photocatalysis-based methane reforming.

Received 21st May 2023
Accepted 5th December 2023

DOI: 10.1039/d3sc02567e

rsc.li/chemical-science

Photocatalysis is a mild technology to reform inert methane into some high-value and active fuels, such as methanol, which has attracted an increasing interest.[1–7] However, the high dissociation energy (439 kJ mol^{-1}) in the cleaving step of the first C–H bond has a high energy barrier which limits the efficiency of the photocatalytic reaction.[8–12] More importantly, these high-value and active fuels are often metastable,[13–17] and are easy to be excessively oxidized into low-value CO or even CO_2.[5,18–20] Considering these issues, many photocatalysts and cocatalysts have been developed to improve yield and selectivity by extending the light-response range, improving charge separation or enhancing catalytic C–H activation. Besides, many studies have also been performed to tune the pathway of the catalytic reaction.[2] For example, gaseous oxygen was used as the oxidant to produce $^{\bullet}OH$ radicals for oxidizing methane into methanol with a high reaction rate of 2.0 mmol g^{-1} h^{-1} in the photocatalytic reaction.[21] However, the selectivity for the targeted products, such as methanol, is often limited to less than 50% though the reaction rate of methane oxidation can be significantly improved by using oxygen as the oxidant.[22] This is directly related to the overoxidation of CH_3OH by the active $^{\bullet}OH$ or $^{\bullet}O_2^-$ radicals, which limits the practical application of photocatalytic methane oxidation.[21,23] Hence, improving the selectivity for the targeted high-value product, without comprising the reaction rate, will be desirable for photocatalytic methane reforming.

Though some semiconductor photocatalysts, such as TiO_2, have a strong oxidizing ability for activating methane, the overoxidation of methane reduces the selectivity for the targeted products.[23] In contrast, some nitrides, such as g-C_3N_4, often exhibit a moderate oxidizing ability, but their stability is deficient.[24] Recently, InGaN photocatalysts with tunable band-edge potentials and surface band structure have been well synthesized by adjusting the In content in the GaN segment,[25,26] which can provide a suitable platform to control the reaction pathway of photocatalytic methane oxidation. Herein, we report a water-assisted photocatalytic methane oxidation process for highly selective methanol production on metallic Ag nanoparticle-loaded InGaN nanowires (Ag/InGaN). The experimental XPS

[a]*Department of Electrical Engineering and Computer Science, University of Michigan, Ann Arbor, MI 48109, USA. E-mail: ztmi@umich.edu*

[b]*Department of Materials Science and Engineering, University of Michigan, 2300 Hayward Street, Ann Arbor, Michigan 48109, USA*

† Electronic supplementary information (ESI) available. See DOI: https://doi.org/10.1039/d3sc02567e

and theoretical PDOS analyses revealed that water molecules adsorbed on AgNPs can promote the electron transfer from InGaN to AgNPs, which enabled the production of highly active Ag species with a lower oxidation state in AgNPs. These Ag species induced by water adsorption were demonstrated to be active and essential for highly selective methanol production according to the *in situ* IR spectrum and the reaction pathway simulation.

InGaN nanowires were prepared on a silicon wafer by plasma-assisted molecular beam epitaxy (PAMBE).[25] The AgNPs were deposited on InGaN nanowires by a typical photoreduction method. The field emission scanning electron microscopy (FESEM) images show that the InGaN nanowires with lengths of ~1.2 μm are well arrayed on a silicon wafer (Fig. 1a). According to the X-ray diffraction (XRD) pattern (Fig. 1b), the crystal structure of the as-prepared sample is assigned to hexagonal InGaN (standard PDF card 2-1078). It should be noted that one main peak at 34.7° and one weak shoulder peak at 34.4° in the XRD pattern are assigned to the GaN and InGaN segments in InGaN/GaN nanowires, respectively. Additionally, the XRD peak of metallic Ag nanoparticles cannot be detected due to its low content. Besides, it is also revealed that InGaN nanowires grow along the [002] direction on the silicon wafer, which is further demonstrated by the high-angle annular dark-field scanning transmission electron microscopy (HAADF-STEM) image (Fig. 1c). A clear lattice fringe with a width of 0.260 nm in the InGaN segment is measured along the growth direction (*c*-axis) of InGaN nanowires. It should be noted that the role of the GaN segment in InGaN nanowires is to stabilize the growth of InGaN segments.[25] Metallic AgNPs with a typical lattice constant of 0.202 nm are observed on the surface of InGaN nanowires (Fig. 1d), and act as the cocatalyst in photocatalysis. The content of AgNPs deposited on InGaN nanowires is determined to be 45.3 μg cm^{-2} according to an inductively coupled plasma-atomic emission spectrometer. The energy dispersive X-ray (EDS) elemental mapping suggests the distribution of AgNPs on the surface of InGaN nanowires as well as the formation of InGaN segments (Fig. 1e). The room-temperature photoluminescence spectrum shows one strong emission peak at 491 nm and one weak peak at 361 nm (Fig. 1f), which are assigned to InGaN segments and GaN segments, respectively.[25,27] This result indicates that the InGaN segments have a band gap of 2.53 eV. Thus, the ratio of In and Ga in InGaN segments was calculated to be 1 : 3 according to the reported formula.[28]

The as-prepared Ag/InGaN sample was used in the water-assisted photocatalytic methane reforming reaction. In a well-designed reaction system (Fig. S1†), the photocatalyst wafer was stabilized on a quartz holder. A water layer at the bottom of chamber provided water vapor for the photocatalytic reaction. CH_4 and O_2 were used as the feed gas for methanol production. First, the ratio of CH_4 and O_2 was optimized in the presence of

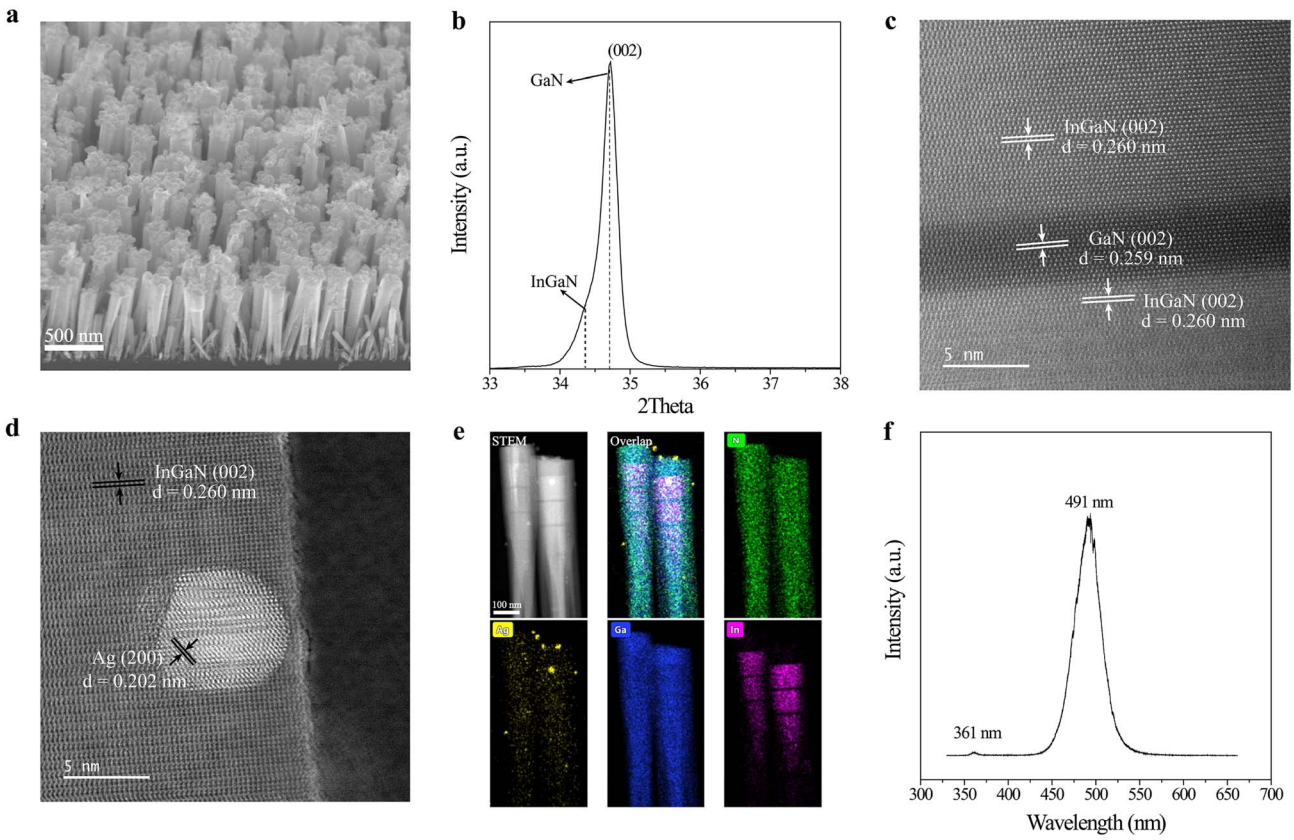

Fig. 1 Structure characterization. (a) A 45°-tilted FESEM image, (b) XRD pattern, (c) HAADF-STEM image, (d) bright-field TEM image, (e) EDS elemental mapping and (f) room-temperature PL spectrum of Ag/InGaN nanowires.

water (Fig. 2a and S2†). The obtained results shows that the highest methanol production rate (21.4 μmol cm^{-2} h^{-1} or 45.5 mmol g^{-1} h^{-1}) is achieved at a ratio of 1 : 1. Meanwhile, a selectivity of 93.3% for methanol production is obtained. The by-products consist of CO and ethane. The control experiment without water demonstrates that the addition of water could increase the methanol production rate by 55 times and selectivity by 9 times, as shown in Fig. 2b. Besides, the activity of pristine InGaN is 12-fold lower than that of Ag/InGaN under the same conditions (Fig. S3†). The above results indicate that the coexistence of water and Ag nanoparticles is significant for the performance improvement of InGaN. As further summarized in Table S1,† the achieved methanol-production activity on Ag/InGaN is nearly one to two orders of magnitude higher than that in the previous reports. Moreover, when replacing H_2O with D_2O, the methanol production rate is observably reduced to ~11.0 μmol cm^{-2} h^{-1}, compared to methane oxidation using H_2O (Fig. 2b), implying the crucial role of H_2O in the present photocatalytic methane oxidation. It should be noted that the decreased activity with D_2O is considered to be from the lower saturated vapor pressure of D_2O than that of H_2O.[29] Further nuclear magnetic resonance (NMR) measurements show that all hydrogen elements of the produced methanol consist of H instead of D from D_2O (Fig. S4†). This result implies that water molecules do not directly react with methanol or oxygen to form the intermediate. Instead, it is considered that the water molecule acts as a molecule "catalyst" in photocatalytic methane reforming. Furthermore, the stability of the photocatalyst can reach 13 cycles (each cycle: 4 hours) in the presence of water (Fig. 2c). Stable operation over 50 hours is significantly better than that of previously reported photocatalytic methane oxidation to methanol (see Table S1†). Besides, a turnover number (TON) of 68 534 was achieved in this stability test. It should be noted that the production rate and selectivity of

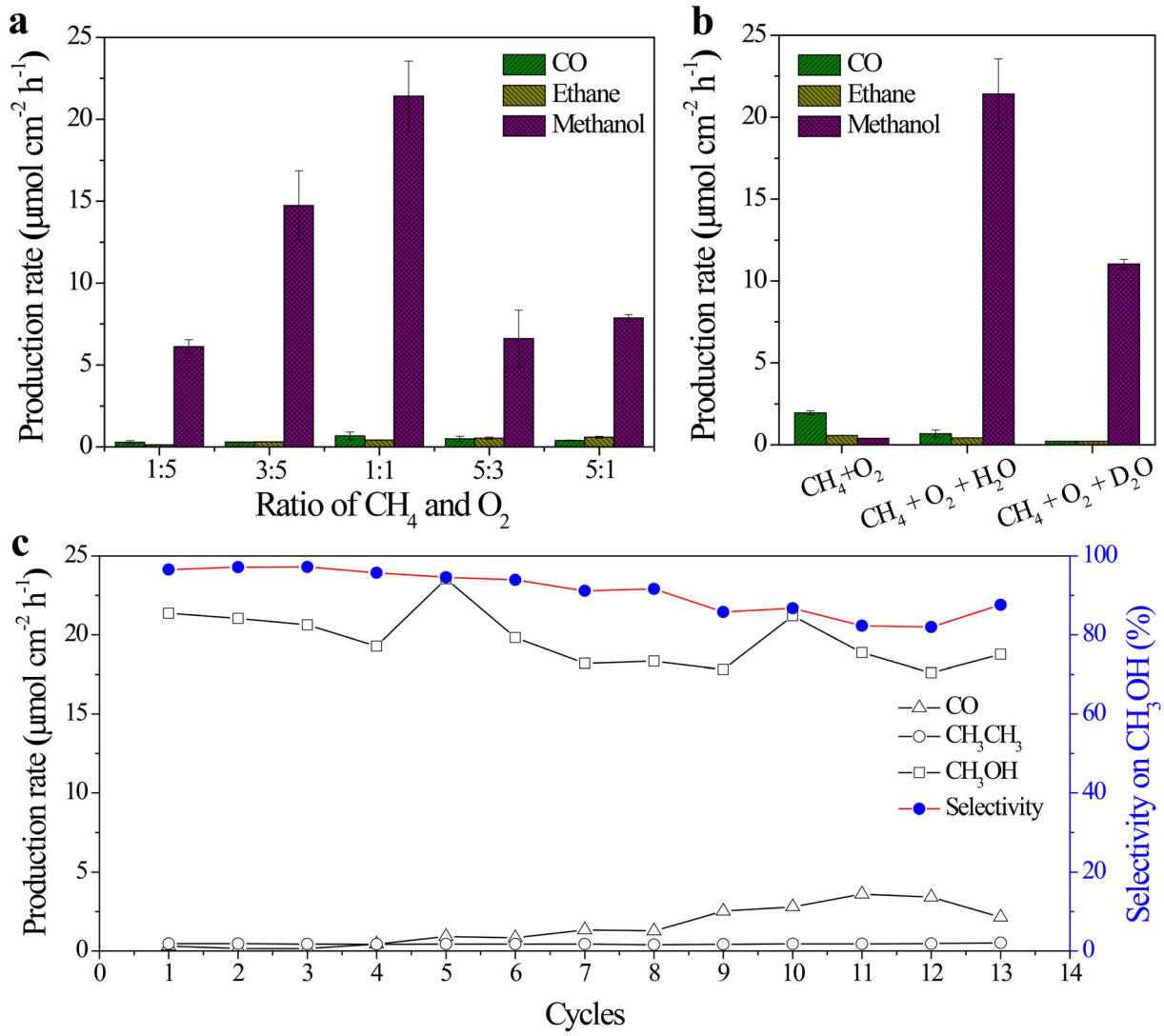

Fig. 2 Performance evaluations. (a) CH_4/O_2 ratio-dependent methane oxidation on the as-prepared Ag/InGaN photocatalyst in the presence of water. (b) Methane oxidation activities of Ag/InGaN without or with H_2O (or D_2O). (c) Stability test of Ag/InGaN under a 300 W Xe lamp with concentrated light of 5000 mW cm^{-2} on a 0.64 cm^2 photocatalyst wafer sample.

methanol were decreased to 9.2 μmol cm^{-2} h^{-1} and 75% at the end of the stability test (Fig. S5†). However, no observable change is observed in the crystal structure of Ag/InGaN after the stability test (Fig. S6 and S7†). The decreased activity and selectivity for methanol is largely due to the aggregation of AgNPs on the InGaN surface according to the FESEM image (Fig. S8†).

To investigate the water promotion effect on the methanol-production activity of Ag/InGaN, the *in situ* infrared diffuse reflectance infrared Fourier transform spectroscopy (DRIFTS) measurements were performed to examine the formation of intermediates. In the absence of water, only a slight change can be observed with reaction time under light irradiation (Fig. 3a). Besides, without irradiation, an IR peak is also not observed in the presence of water (Fig. S9†). However, with the addition of water, an observable peak appears in the range of 925–1600 cm^{-2} under light irradiation, assigned to the C–O bond (Fig. 3b).[30,31] This result indicates that water can significantly promote the photocatalytic oxidation of methane. Besides, methane oxidation is significantly reduced in the absence of Ag nanoparticles (Fig. S10†). This suggests that the coexistence of water and Ag nanoparticles is necessary for photocatalytic methane oxidation on InGaN, which is consistent with the result of the above activity test. Moreover, the high-resolution XPS spectra of Ag/InGaN (Ag/

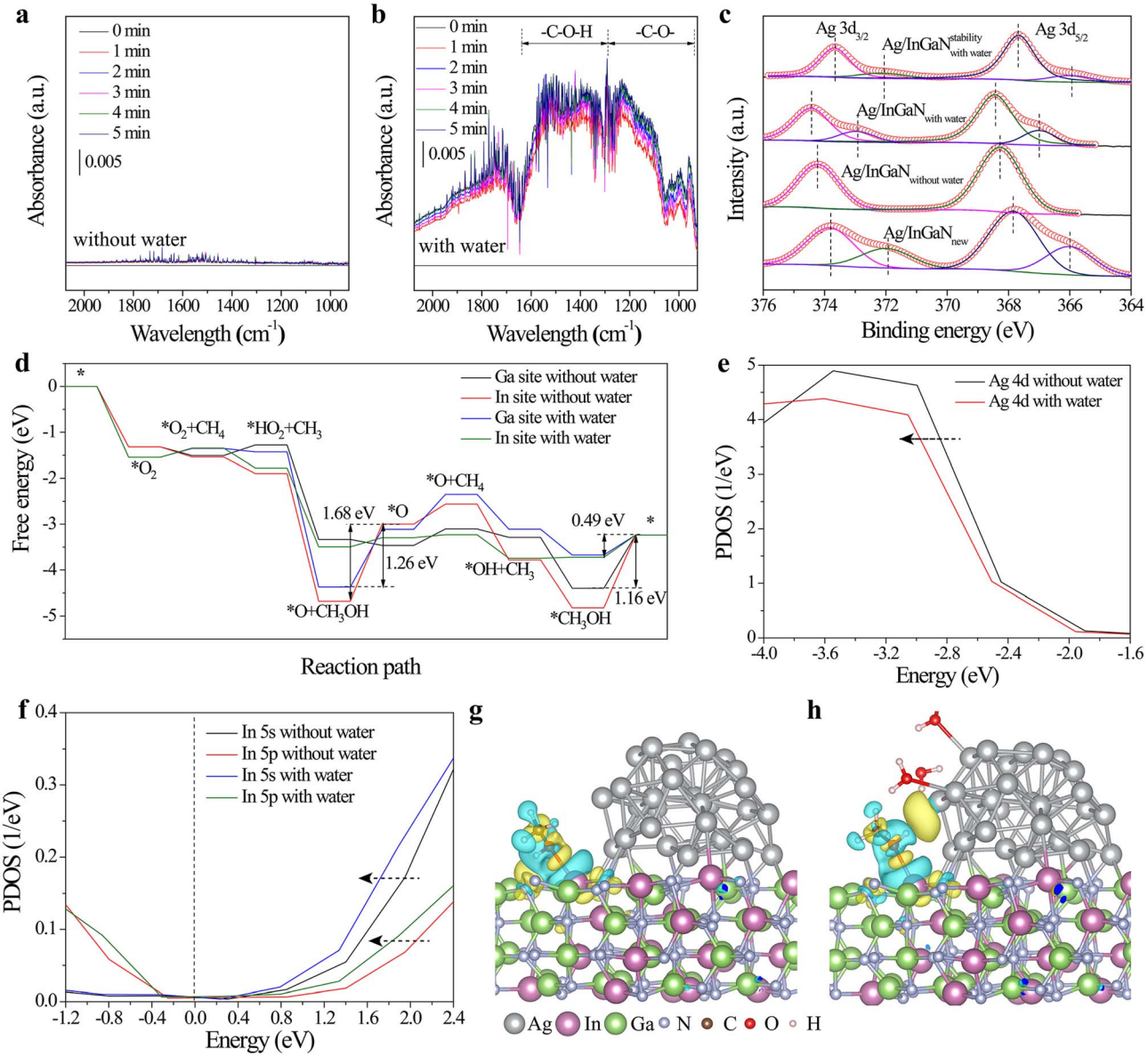

Fig. 3 *In situ* IR spectrum of photocatalytic methane oxidation on Ag/InGaN (a) without or (b) with water. (c) High-resolution XPS spectra of Ag/InGaN before and after the reaction. The circles stand for the fitting curve. (d) Free energy profile of methane oxidation on Ag/InGaN without or with water. (e) PDOS plots of Ag 4d states without or with water. (f) PDOS plots of In 5s and 5p states without or with water. The vertical dashed line stands for the Fermi level. The charge density difference mappings between methanol and Ag/InGaN surfaces (g) without or (h) with water. The isosurface of charge density is 0.005 e $Å^{-3}$. The yellow and sky-blue regions stand for the positive and negative charges, respectively.

$InGaN_{new}$) before the reaction show that two kinds of Ag species exist on AgNPs directly obtained from photoreduction (Fig. 3c). Specifically, the Ag species with a lower oxidation state is observed at 371.9 eV. Interestingly, this peak disappears in Ag/InGaN after one-cycle of methane oxidation without water addition ($Ag/InGaN_{without\ water}$). In contrast, one additional peak can still be found in the more negative region of the Ag 3d XPS spectrum of $Ag/InGaN_{with\ water}$ obtained from one-cycle of water-assisted methane oxidation. This suggests that water can stabilize these Ag species with a lower oxidation state. It should be noted that these Ag species with a lower oxidation state unavoidably decreased with reaction time due to the oxidation or deactivation of Ag nanoparticles. Especially after 16 cycles, only one weak peak can be observed at 372.1 eV in Ag/InGaN after stability test without water. Considering the activity trend, it is speculated that these Ag species with a lower oxidation state are the main active centers for photocatalytic methane oxidation.

To further verify the above provided mechanism, the density functional theory (DFT) simulations were performed to investigate the water promotion effects on photocatalytic methane reforming into methanol. Considering the different work functions of noble metal AgNPs and the InGaN semiconductor,[32] the AgNPs act as the cocatalyst for reducing the adsorbed oxygen into active oxygen species for the activation of methane. Besides, the holes left on InGaN combine with the formed oxygen species to synergistically catalyze methane oxidation. The free energy profile of the catalytic reaction pathway shows that the desorption of methanol is the rate-determining step (Fig. 3d). Specifically, the existence of water significantly decreases the energy barrier of methanol desorption from the photocatalyst surface. The existence of water effectively enables the formation energy of a C–O bond between $*CH_3$ and $*HO_2$ or *OH less negative, which avoids the excessively strong interaction between the formed methanol and catalyst surface. As a result, the addition of water promotes the formation of free methanol molecules. It should be noted that the surface indium (In) site in InGaN is the more active site for methanol production compared to the surface gallium (Ga) site (Fig. 3d). Moreover, the projected density of states (PDOS) of Ag 4d states show that the presence of water shifts Ag 4d states of AgNPs toward a more negative region (Fig. 3e), indicating that water-adsorbed AgNPs obtain more electrons from InGaN and have a lower oxidation state. Furthermore, it is revealed that the surface In site neighboring a AgNP also has a lower oxidation degree in the presence of water (Fig. 3f), which is beneficial for inhibiting the excessive oxidation of the formed methanol into CO. This is further demonstrated by the calculated charge density difference mappings between the formed methanol and photocatalyst surface. The results show that the presence of water changes the adsorption state of methanol on the photocatalyst surface. In the absence of water, the formed methanol only interacts with the InGaN surface (Fig. 3g). However, with the addition of water, methanol is located between InGaN and AgNPs (Fig. 3h). This co-interaction between methanol and InGaN/AgNP can effectively inhibit the inert adsorption of methanol, which is beneficial for the desorption of the formed methanol during the catalytic reaction. This is further demonstrated by the *in situ* IR test of methanol desorption with or without water (Fig. S11†). The result shows that the addition of water can accelerate the desorption of methanol. Hence, it can be concluded that water can tune the electronic states of Ag/InGaN and produce more active surface sites for photocatalytic methane oxidation into methanol.

Data availability

Supporting data of this study are available within the paper. Further details regarding the data are available from the corresponding author upon reasonable request.

Author contributions

P. Z. designed the photocatalyst and performed the photocatalytic reactions. I. N. synthesized GaN NWs. Y. X. and K. S. performed SEM and TEM. P. Z., S. T. and Z. Y. performed the photocatalytic experiments. Z. M. supervised the whole project. P. Z. and Z. M. wrote the manuscript with input from all authors.

Conflicts of interest

Some IP related to this work has been licensed to NS Nanotech, Inc. and NX Fuels, Inc., which were co-founded by Z. M. The University of Michigan and Mi have a financial interest in both companies.

Acknowledgements

This work was supported by United States Army Research Office Award W911NF2110337. The authors also acknowledge the financial support from the University of Michigan College of Engineering and NSF grant #DMR-0723032, and technical support from the Michigan Center for Materials Characterization.

Notes and references

1 L. Zhou, J. M. P. Martirez, J. Finzel, C. Zhang, D. F. Swearer, S. Tian, H. Robatjazi, M. Lou, L. Dong, L. Henderson, P. Christopher, E. A. Carter, P. Nordlander and N. J. Halas, *Nat. Energy*, 2020, **5**, 61–70.
2 X. Y. Li, C. Wang and J. W. Tang, *Nat. Rev. Mater.*, 2022, **7**, 617–632.
3 Y. Y. Fan, W. C. Zhou, X. Y. Qiu, H. D. Li, Y. H. Jiang, Z. H. Sun, D. X. Han, L. Niu and Z. Y. Tang, *Nat. Sustain.*, 2021, **4**, 509–515.
4 S. Q. Wu, X. J. Tan, J. Y. Lei, H. J. Chen, L. Z. Wang and J. L. Zhang, *J. Am. Chem. Soc.*, 2019, **141**, 6592–6600.
5 S. Shoji, X. Peng, A. Yamaguchi, R. Watanabe, C. Fukuhara, Y. Cho, T. Yamamoto, S. Matsumura, M.-W. Yu, S. Ishii, T. Fujita, H. Abe and M. Miyauchi, *Nat. Catal.*, 2020, **3**, 148–153.

6 X. Yu, V. L. Zholobenko, S. Moldovan, D. Hu, D. Wu, V. V. Ordomsky and A. Y. Khodakov, *Nat. Energy*, 2020, **5**, 511–519.
7 Z. Chen, S. Wu, J. Ma, S. Mine, T. Toyao, M. Matsuoka, L. Wang and J. Zhang, *Angew. Chem., Int. Ed.*, 2021, **60**, 11901–11909.
8 Y. Wang, P. Hu, J. Yang, Y.-A. Zhu and D. Chen, *Chem. Soc. Rev.*, 2021, **50**, 4299–4358.
9 V. L. Sushkevich, D. Palagin, M. Ranocchiari and J. A. van Bokhoven, *Science*, 2017, **356**, 523–527.
10 L. C. Buelens, V. V. Galvita, H. Poelman, C. Detavernier and G. B. Marin, *Science*, 2016, **354**, 449–452.
11 W. Huang, A. C. Johnston-Peck, T. Wolter, W.-C. D. Yang, L. Xu, J. Oh, B. A. Reeves, C. Zhou, M. E. Holtz, A. A. Herzing, A. M. Lindenberg, M. Mavrikakis and M. Cargnello, *Science*, 2021, **373**, 1518–1523.
12 Z. Liu, E. Huang, I. Orozco, W. Liao, R. M. Palomino, N. Rui, T. Duchon, S. Nemsak, D. C. Grinter, M. Mahapatra, P. Liu, J. A. Rodriguez and S. D. Senanayake, *Science*, 2020, **368**, 513–517.
13 M. A. Newton, A. J. Knorpp, V. L. Sushkevich, D. Palagin and J. A. van Bokhoven, *Chem. Soc. Rev.*, 2020, **49**, 1449–1486.
14 Z. Guo, B. Liu, Q. Zhang, W. Deng, Y. Wang and Y. Yang, *Chem. Soc. Rev.*, 2014, **43**, 3480–3524.
15 W. X. Huang, S. R. Zhang, Y. Tang, Y. T. Li, L. Nguyen, Y. Y. Li, J. J. Shan, D. Q. Xiao, R. Gagne, A. I. Frenkel and F. Tao, *Angew. Chem., Int. Ed.*, 2016, **55**, 13441–13445.
16 S. Chen, J. Zaffran and B. Yang, *Appl. Catal., B*, 2020, **270**, 118859.
17 Z. X. Xi, B. J. Zhou, Y. Yu, B. B. Jiang, Z. W. Liao, J. D. Wang, Z. L. Huang, Y. Yang, J. Y. Sun and Y. R. Yang, *Catal. Sci. Technol.*, 2020, **10**, 6161–6172.
18 H. Song, X. Meng, Z.-j. Wang, Z. Wang, H. Chen, Y. Weng, F. Ichihara, M. Oshikiri, T. Kako and J. Ye, *ACS Catal.*, 2018, **8**, 7556–7565.
19 S. Song, H. Song, L. Li, S. Wang, W. Chu, K. Peng, X. Meng, Q. Wang, B. Deng, Q. Liu, Z. Wang, Y. Weng, H. Hu, H. Lin, T. Kako and J. Ye, *Nat. Catal.*, 2021, **4**, 1032–1042.
20 J. J. Xie, R. X. Jin, A. Li, Y. P. Bi, Q. S. Ruan, Y. C. Deng, Y. J. Zhang, S. Y. Yao, G. Sankar, D. Ma and J. W. Tang, *Nat. Catal.*, 2018, **1**, 889–896.
21 H. Song, X. Meng, S. Wang, W. Zhou, X. Wang, T. Kako and J. Ye, *J. Am. Chem. Soc.*, 2019, **141**, 20507–20515.
22 P. Zhou, I. A. Navid, Y. Xiao, Z. Ye, W. J. Dong, P. Wang, K. Sun and Z. Mi, *J. Phys. Chem. Lett.*, 2022, **13**, 8122–8129.
23 N. Feng, H. Lin, H. Song, L. Yang, D. Tang, F. Deng and J. Ye, *Nat. Commun.*, 2021, **12**, 4652.
24 Y. Y. Zhou, L. Zhang and W. Z. Wang, *Nat. Commun.*, 2019, **10**, 506.
25 M. G. Kibria, F. A. Chowdhury, S. Zhao, B. AlOtaibi, M. L. Trudeau, H. Guo and Z. Mi, *Nat. Commun.*, 2015, **6**, 6797.
26 P. Zhou, I. A. Navid, Y. Ma, Y. Xiao, P. Wang, Z. Ye, B. Zhou, K. Sun and Z. Mi, *Nature*, 2023, **613**, 66–70.
27 M. G. Kibria, H. P. T. Nguyen, K. Cui, S. Zhao, D. Liu, H. Guo, M. L. Trudeau, S. Paradis, A.-R. Hakima and Z. Mi, *ACS Nano*, 2013, **7**, 7886–7893.
28 P. G. Moses and C. G. V. d. Walle, *Appl. Phys. Lett.*, 2010, **96**, 021908.
29 F. T. Miles and A. W. C. Menzies, *J. Am. Chem. Soc.*, 1936, **58**, 1067–1069.
30 A. Koishybay and D. F. Shantz, *J. Am. Chem. Soc.*, 2020, **142**, 11962–11966.
31 Y. Yang, Z. Chai, X. Qin, Z. Zhang, A. Muhetaer, C. Wang, H. Huang, C. Yang, D. Ma, Q. Li and D. Xu, *Angew. Chem., Int. Ed.*, 2022, **61**, e202200567.
32 J. H. Yang, D. G. Wang, H. X. Han and C. Li, *Acc. Chem. Res.*, 2013, **46**, 1900–1909.